One-Step Sub-10 μm Patterning of Carbon-Nanotube Thin Films for Transparent Conductor Applications

Norihiro Fukaya,[†] Dong Young Kim,[‡] Shigeru Kishimoto,[†] Suguru Noda,[‡] and Yutaka Ohno[†,*]

[†]Department of Quantum Engineering, Nagoya University, Furo-cho, Chikusa-ku, Nagoya 464-8603 Japan and [‡]Department of Applied Chemistry, Waseda University, 3-4-1 Okubo, Shinjuku-ku, Tokyo, 169-8555 Japan

ABSTRACT

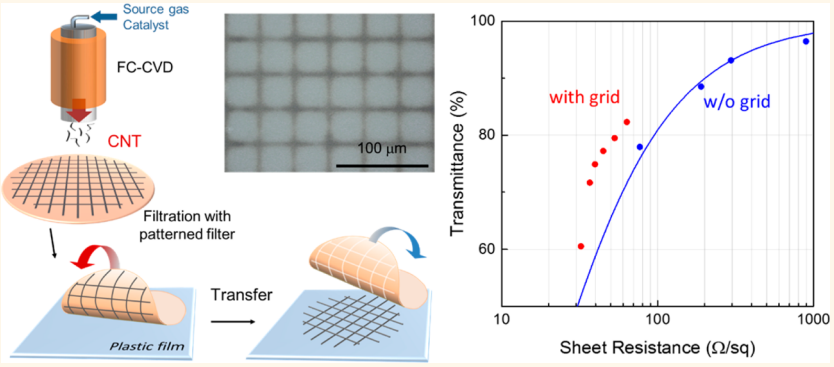

We propose a technique for one-step micropatterning of as-grown carbon-nanotube films on a plastic substrate with sub-10 μm resolution on the basis of the dry transfer process. By utilizing this technique, we demonstrated the novel high-performance flexible carbon-nanotube transparent conductive film with a microgrid structure, which enabled improvement of the performance over the trade-off between the sheet resistance and transmittance of a conventional uniform carbon-nanotube film. The sheet resistance was reduced by 46% at its maximum by adding the microgrid, leading to a value of 53 Ω/sq at a transmittance of 80%. We also demonstrated easy fabrication of multitouch projected capacitive sensors with 12 × 12 electrodes. The technique is quite promising for energy-saving production of transparent conductor devices with 100% material utilization.

KEYWORDS: carbon nanotube · micropatterning · transparent conductive film · touch sensor · flexible

Transparent conductive films (TCFs) are widely used in most flat-panel displays (FPDs) such as liquid-crystal displays and recently in organic light-emitting diode displays and touch sensors, which have been fabricated on glass traditionally. Carbon-nanotube (CNT) TCFs[1−7] are attracting considerable attention in the FPD industry because they potentially have excellent conductivity originating from the long mean free path of carriers,[8,9] and they are also free from the resource and price fluctuation problems[10] that sometimes arise for indium−tin−oxide (ITO) conventionally used in FPDs as TCFs. In addition, CNT TCFs also have various advantages in mechanical flexibility,[11] chemical stability, lower refractive index, less color tone and haze,[12] and so on, compared to ITO and recent silver-nanowire-based TCFs. CNT thin films are quite promising material for not only FPD applications but also flexible device applications[13−15] such as e-papers and e-signages fabricated on a plastic film, which will be commercialized in the near future. While graphene may also have similar advantages in physical properties,[16,17] they need to be grown on a metal template such as a copper foil by chemical vapor deposition (CVD) and then transferred onto a target substrate,[18,19] which increases manufacturing cost as a result. The excellent processability of CNT films can realize ultimately low-cost manufacturing of TCFs based on nonvacuum and low-temperature processes such as solution-based coating[3,20,21] and dry transfer[7,22] processes.

* Address correspondence to yohno@nuee.nagoya-u.ac.jp.

Received for review August 12, 2013 and accepted March 27, 2014.

Published online April 01, 2014
10.1021/nn4041975

Much effort has been expended on reducing the sheet resistance of CNT TCFs, which are currently still higher than those of ITO,[23,24] graphene,[19] and metal nanowires.[25] It is known that the junction resistance between each CNT is much higher than the resistance of the CNT itself, and the conductivity of a CNT TCF is dominated by the tube-to-tube junction resistance,[26−29] that is, the longer the CNTs and the lower the number of tube-to-tube junctions in a current pathway, the lower the sheet resistance. Contamination of CNTs may also contribute to higher tube-to-tube junction resistance. Recently, high-performance CNT TCFs using long and clean CNTs have been reported.[7,22] In these studies, CNTs grown by floating catalyst chemical vapor deposition (FC-CVD)[30] were collected by a membrane filter and then transferred onto an objective substrate. It has been demonstrated that the dry transfer process is quite easy and can form a CNT film quickly on various kinds of substrate such as plastic films, metal foils, and Si wafer. The performance, that is, the sheet resistance and optical transmittance, is comparable to that of ITO deposited on plastic.

However, the most critical problem of CNT TCFs is the existence of a trade-off between the sheet resistance and transmittance, originating from the finite absorbance of CNTs. As the thickness of a CNT thin film increases, the transmittance decays exponentially, whereas the sheet resistance decreases inversely proportionally; as a consequence, the trade-off relationship is expressed by the equation

$$T = \exp\left(-\frac{\alpha\rho}{R}\right) \quad (1)$$

where T and R are the transmittance and sheet resistance, respectively, of a CNT TCF; ρ and α are the resistivity and absorption coefficient, respectively, of the CNT film material. In order to further improve the performance of CNT TCFs, it is important to overcome the trade-off as well as improve the quality of CNT materials.

For the device application of CNT TCFs, patterning of a thick CNT film is one of the key processes. So far, etching processes with oxygen plasma[31,32] and with ozone[33−35] combined with a lithography technique are often used. However, the production throughput of such techniques is low, and the resulting conductivity is also low due to the contamination of CNTs by the photoresist. Moreover, the substrate may be damaged by the etching process, especially in the case of plastic substrates with weak heat tolerance and low etching selectivity to CNTs. Direct patterning with printing technologies such as microcontact,[20,36] screen,[37] and inkjet[38−40] printings have been reported for the fabrication of CNT electrodes; however, these techniques take extremely long periods of time to form a CNT film with a practical thickness. Device applications require simple and quick patterning techniques with neither contamination nor damage to both CNTs and the substrate.

In this work, we propose the technique for one-step sub-10 μm patterning of as-grown CNT films on a plastic substrate based on the dry transfer process, using the membrane filter on which resist patterns are formed. By utilizing this technique, we demonstrated the novel high-performance flexible CNT TCFs with a microgrid structure, which enabled us to overcome the trade-off between sheet resistance and transmittance of conventional CNT TCFs. We also demonstrated easy fabrication of multitouch projected capacitive sensors with 12 × 12 electrodes.

RESULTS AND DISCUSSION

To realize micropatterning of clean and long CNTs, we employed the dry transfer method based on the FC-CVD technique,[7] using the membrane filter on which resist patterns were formed by the lithography process, as shown in Figure 1a. The CNTs were grown by FC-CVD, collected with the patterned membrane filter, and then transferred onto a target substrate (see Methods section for details on the CNT growth; movie S1 of the transfer process for CNT micropatterns is available in Supporting Information). To achieve the lithography on the membrane filter without penetration of photoresist into the filter, we used filters made of polyvinylidenedifluoride (PVDF) with a pore size of 0.45 μm (Millipore HVHP04700) that is rather hydrophobic and more solvent-resistant than other commercially available membrane filters. We also carried out the fluoridation treatment by exposing the filter to CF_4 plasma to enhance the hydrophobicity of the membrane filter (see Methods section).

Previously, Lim *et al.* reported a technique to form CNT patterns on PDMS (polydimethylsiloxane) with a patterned filter based on vacuum filtration of water suspension of CNTs and transfer process;[41] however, the transfer process is destructive for the patterned filter, and particular types of target substrate is needed such as PDMS. Because the CNTs are tightly attached to the filter due to the surface tension of the solution in the case of the solution-based filtration method, the transfer of the CNTs is achieved by coating precursor solution of the substrate material and subsequent curing. In contrast to the previous method, the patterned membrane filter can be used multiple times for the filtration and transfer process in the case of the present technique (Supporting Information Figure S1). Moreover, CNTs are transferable onto various kinds of substrates even onto electron devices to be integrated. The electrical conductivity of the CNTs is not degraded by the pattering process because long and clean as-grown CNTs are directly deposited in the form of the CNT patterns.

Figure 1b shows the microgrid pattern of the photoresist formed lithographically on the membrane filter.

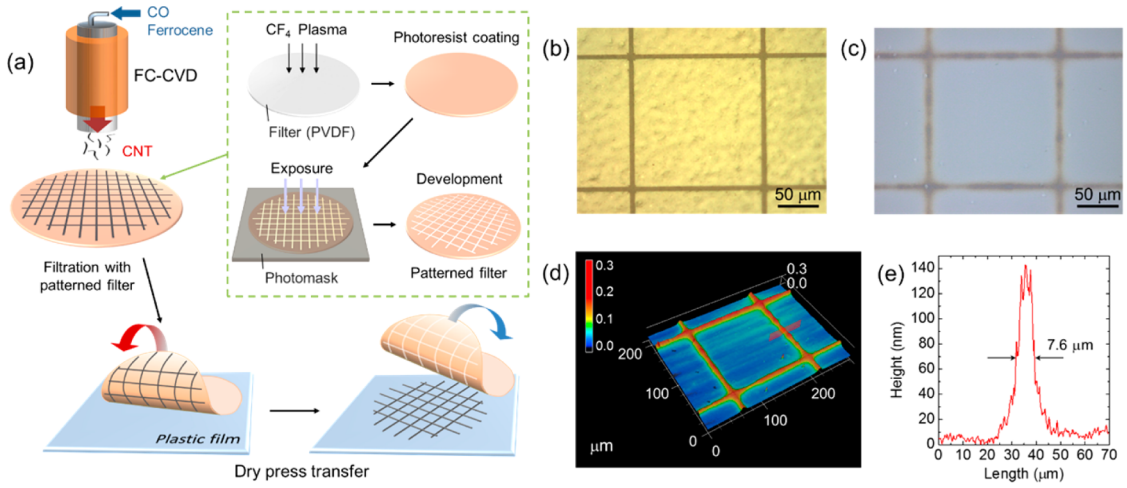

Figure 1. (a) Schematic of the micropatterning process based on the dry transfer method with a micropatterned membrane filter. CNTs were grown by FC-CVD, collected with a micropatterned membrane filter, and transferred onto the objective substrate. The process to fabricate the patterned membrane filter is also shown in the box enclosed by the dashed green line. After exposing CF_4 plasma to the filter to ensure the hydrophobicity, a normal lithographic process is performed on the filter. The patterned filter can be used multiple times in the transfer process. Micrographs of (b) the membrane filter with a photoresist pattern and (c) a micropattern of CNTs formed on a plastic film. (d) Topographic image of the micropattern measured by laser microscope. (e) Cross-sectional profile measured by a laser microscope. The cross section was measured along the red plane in (d).

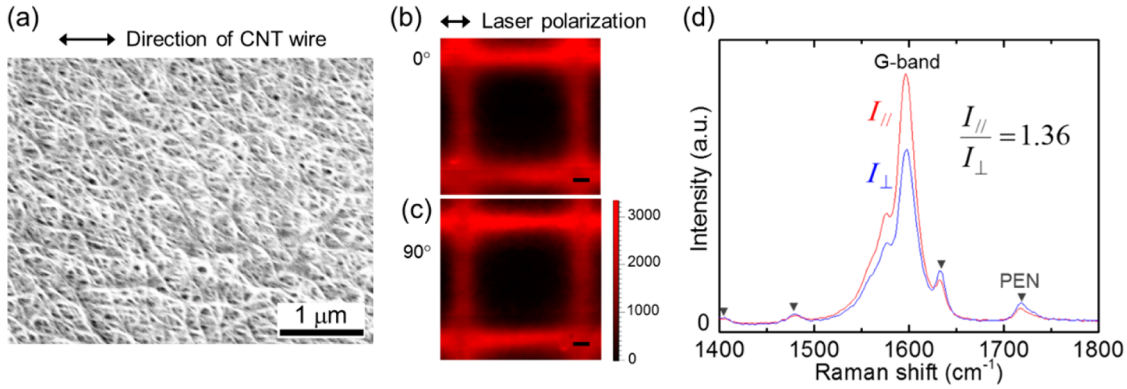

Figure 2. (a) SEM image of CNTs in the microgrid. (b,c) Spatial distributions of G-band intensity of Raman scattering measured for the CNT grid. The scale bar is 10 μm. The sample was rotated by 90° in the case of (c). (d) Raman scattering spectra measured at two positions where CNT wire is parallel ($I_{//}$) or perpendicular ($I_{\perp}$) to polarization of the excitation laser. The peaks denoted by a triangle originate from the PEN substrate.

Using this patterned membrane filter, the microgrid pattern of CNTs was successfully formed on the plastic film (Figure 1c,d) by the dry transfer technique. Densification of the CNT film with isopropyl alcohol (IPA) was carried out (see Methods section). The full width at half-maximum of the CNT wire was 7.6 μm, as shown in Figure 1e, which was much smaller than those formed using metal masks (>100 μm) in previous works.[7,42] It is worth mentioning that the resolution recognizable for human eyes is in the range of 300−400 dpi, which corresponds to ~70 μm in size. This means that the CNT micropatterns formed by this technique are hardly recognized by the naked eye and are therefore suitable for TCF device applications, as described later.

The widths of the obtained CNT microgrid wires were considerably wider than those designed on the photomask; for example, the obtained line width was 7.6 μm, while that designed on the photomask was 3 μm. This was mainly caused by the CNTs adhering on the photoresist surface around the openings during CNT collection by the patterned membrane filter. The amount of CNTs adhering onto the photoresist can be decreased by functionalizing the surface of the photoresist.

SEM observation and micro-Raman measurements were carried out to characterize the microscopic structure of the CNT microgrid. Figure 2a shows the SEM image of the CNTs. The CNTs seem to be uniformly deposited, and no significant correlation between the direction of each CNT and that of the CNT wire was found. In the micro-Raman measurements, on the other hand, the results show that the CNTs are slightly aligned in the direction along the CNT wires. We measured spatial distributions of G-band intensity

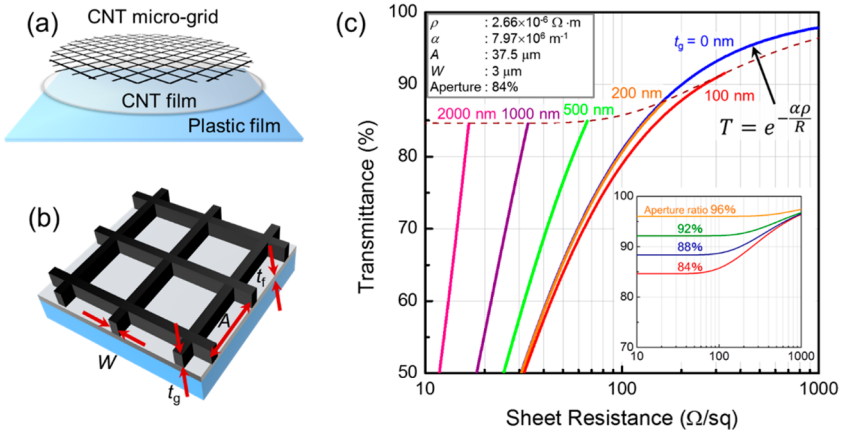

Figure 3. (a) Schematic of proposed CNT TCF with a microgrid structure, (b) structural parameters of the TCF, and (c) simulated $T-R$ curves for various values of t_g. The blue curve represents $t_g = 0$; *i.e.*, it shows the trade-off relationship of conventional uniform CNT TCFs. The dashed curve shows the maximum transmittances for an aperture ratio of 84%. The top-left inset shows parameters used in the simulation. The bottom-right inset shows the maximum transmittance curves for various aperture ratios.

of Raman scattering with a linearly polarized excitation laser for the CNT microgrid (see Methods section for Raman scattering measurement). A higher Raman intensity was observed for the CNT wires parallel to the laser polarization ($I_{\parallel}$), compared to those perpendicular ($I_{\perp}$), as can be seen in Figure 2b. The same result was obtained when the sample was rotated by 90° (Figure 2c). The intensity ratio $I_{\parallel}/I_{\perp}$ at G-band was 1.36, as shown in Figure 2d, suggesting a possibility of alignment of CNTs along the direction of the CNT wire. Because the length of CNTs and their bundles exhausted from the FC-CVD is longer than the width of line-shaped openings of the photoresist mask on the membrane filter, there would be a possibility that CNTs are aligned in the direction along the line-shaped openings by the gas flowing through the openings. However, at these high CNT densities, the small degree of alignment does not significantly affect the conductivity of the CNT microgrid.

Using the micropatterning technique, we propose a novel CNT TCF with a microgrid structure, as shown in Figure 3a, as a method to overcome the trade-off between the sheet resistance and transmittance of CNT TCFs. The TCF consists of a double layer with a uniform CNT thin film and the microgrid. The microgrid plays a role in reducing the sheet resistance of the TCF, while the transmittance is not significantly reduced if the width of the microgrid wires is thin enough when compared to the period of the microgrid.

First, a performance estimation was carried out with a simple continuum model, as shown in Figure 3b. Here, we assume a rectangular cross section of the wire of the CNT film and a constant resistivity (ρ) of the CNT film; that is, the resistivity does not depend on the width, thickness, or length of the CNT film. We also assume that the cross section of a wire of the grid is rectangular. The sheet resistance of the TCF with the grid (R) is given by the parallel connection of sheet resistances of the uniform CNT film (R_f) and CNT grid (R_g):

$$R = \left(\frac{1}{R_f} + \frac{1}{R_g}\right)^{-1} \approx \rho\left(t_f + \frac{W}{A}t_g\right)^{-1} \qquad (2)$$

where t_g and t_f are the thicknesses of the grid and uniform film, respectively, W is the width of a grid wire, and A is the period of the grid. The validity of this expression was confirmed by simulation based on finite element method (see Supporting Information). The optical transmittance is given by the product of those of the uniform film and the grid as follows:

$$T = T_g T_f = \left[\left(\frac{A-W}{A}\right)^2 + \frac{W(2A-W)}{A^2}e^{-\alpha t_g}\right]e^{-\alpha t_f} \qquad (3)$$

The first and second terms on the right correspond to the transmittances of the opening and grid, respectively. If the CNT grid wire is thick enough, the second term is negligible, and then T is simply determined by the aperture ratio and transmittance of the uniform CNT film. Here, the aperture ratio is the area of opening of the microgrid per unit area, $[(A-W)/A]^2$.

The calculated transmittances as a function of sheet resistance for various t_g values ($T-R$ curves) are shown by solid curves in Figure 3c. Here, we employed the values shown in the top-left inset. The values of ρ and α used in the calculation were typical values of CNT films grown by our group (see Supporting Information for the method to evaluate ρ and α). The blue curve is for uniform CNT TCFs ($t_g = 0$) with various t_f values, representing the trade-off relationship between the transmittance and sheet resistance given by eq 1. By adding the grid to the uniform film, the $T-R$ curve shifted toward lower sheet resistance; that is, the sheet resistance could be significantly reduced over the limit

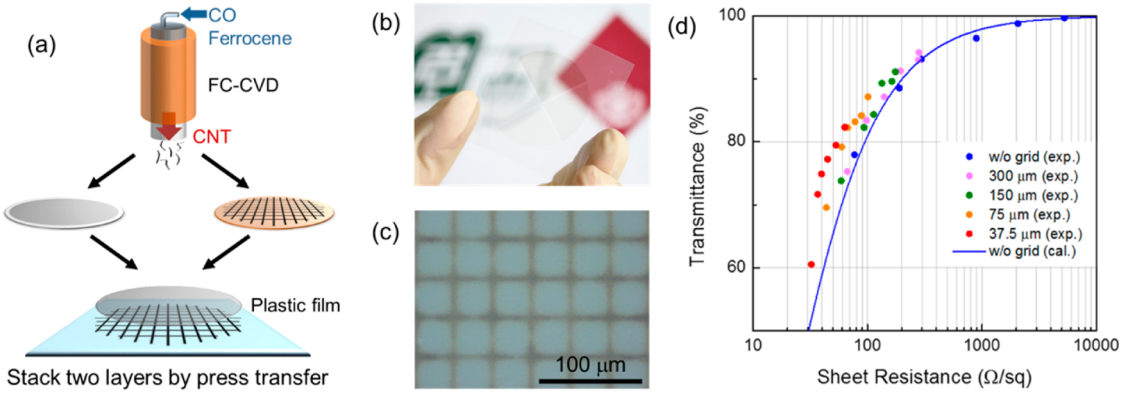

Figure 4. (a) Schematic of fabrication process for CNT TCFs with a microgrid. CNTs grown by FC-CVD are collected by a normal membrane filter and a patterned one, separately, and then stacked onto a PEN film by the transfer process. (b) Photograph of a fabricated CNT TCF with a microgrid. The sample contained four regions with different grid periods. (c) Micrograph of the TCF with a microgrid with a period of 37.5 μm. (d) Transmittance *versus* sheet resistance of CNT TCFs with the microgrid for various periods of the grid. The blue dots and curve, respectively, represent the experimental data and the fitting curve by eq 1 for uniform CNT TCFs without the grid, showing the trade-off relationship of a conventional CNT TCF.

that arises from the trade-off. The dashed curve shows the maximum transmittance curve, which was drawn by connecting the highest transmission obtained at $t_f = 0$ for each t_g. Namely, the dashed curve shows the transmittance as a function of sheet resistance only of microgrids (*i.e.*, $t_f = 0$) for various t_g values. With increasing t_g above 200 nm, the maximum transmittance reached the same value as the aperture ratio of the grid. The larger t_g, the lower R. Moreover, by increasing the aperture ratio, the maximum transmittance can increase above 95%, as shown in the bottom-right inset of Figure 3c.

We fabricated the double-layered CNT TCFs by utilizing the micropatterning technique based on the dry transfer process, as shown in Figure 4a. The uniform CNT film and CNT microgrid were both formed on a polyethylenenaphthalete (PEN) film with a thickness of 100 μm (Teijin DuPont Films, Q65FA) by the transfer process. Densification with IPA and chemical doping with HNO_3[5] was then carried out (see Methods section). Figure 4b,c shows a photograph and micrograph, respectively, of the CNT TCF with the microgrid. Four types of TCFs with different grid periods of 37.5, 75, 150, and 300 μm were formed on a 50 $\times$ 50 mm^2 specimen. The microgrid structure was invisible to the naked eye for a grid period of <75 μm, as expected. This agrees with the recognizable resolution for the human eye described earlier.

The sheet resistance was measured by the four-probe technique with a correction factor of $\pi/(\ln 2)$. Since the period of the grid was small enough compared to the distance between the probes, we can assume an electrically uniform film for the current CNT TCFs with the grid. The measurement of transmittance was carried out, avoiding disturbance from the microstructure of the grid. Figure 4d shows the transmittance at a wavelength of 550 nm *versus* sheet resistance for various periods of microgrid. For each case, six samples with different thicknesses of the uniform CNT film were prepared. Blue dots and curve, respectively, represent the experimental data and the fitting curve by eq 1 for the uniform CNT TCFs without the grid; that is, the blue curve shows the trade-off of conventional CNT TCFs. Here, the fitting parameter that gives the best fit is $\alpha\rho = 21.2$, which agrees with experimentally measured values of α and ρ shown in the inset of Figure 3c. By adding the grid, the performances of CNT TCFs were improved over the trade-off curve. The sheet resistance at a transmittance of 80% was reduced by 46% from 95 to 53 Ω/sq by adding the grid with a period of 37.5 μm. This value was among the best data for CNT TCFs.[5,7,21,22,43−45]

Comparisons between the experimental data and model calculation (see Supporting Information) show a discrepancy in sheet resistance, whereas good agreement was obtained in transmittance. The experimentally obtained sheet resistance suggests that the resistivity of the grid structure is lower than that of the uniform film, even though the quality of CNTs is same. This might be due to the densification process in which surface tension of liquid depends on the structure of the CNT film. Further study is necessary to clarify this point.

At present, the thickness of the CNT microgrid is limited up to ~150 nm after the densification. This is because CNTs eventually deposit around the opening of the photoresist after the resist opening is filled by CNTs. The maximum thickness would be able to be increased by increasing the thickness of the photoresist formed on the filter. Although a small amount of CNTs may also be deposited on the photoresist and transferred onto the objective substrate, the influence on optical transmission of the TCFs with the microgrid is negligible.

A bending test was performed to demonstrate the flexibility of the current CNT TCFs with the microgrid.

The two-terminal resistance was measured between two gold electrodes formed on the TCF, as shown in the inset of Figure 5. The sample was attached onto various cylindrical glass tubes with different diameters. The variation in resistance ($\Delta R/R_0$) is plotted in Figure 5 (red circles) as a function of strain on the surface of the plastic substrate. Here, the strain was evaluated by $t/2r$, where t is the thickness of the substrate and r is the radius of curvature.[46] The variation in resistance was less than 5% for a strain of 2%, which was comparable to those of conventional uniform CNT TCFs.[47] The variation in resistance was elastic; that is, the resistance returned to the initial value when the sample was released and remained flat for the strain up to at least 1.7%, as shown by the black open circles in Figure 5.

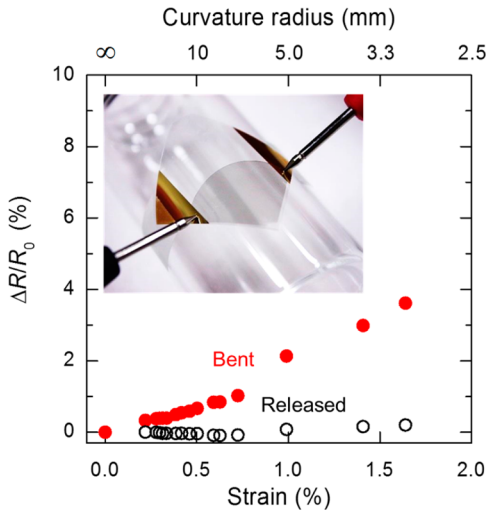

Figure 5. Variation in resistance normalized by the initial value as a function of tensile strain (red circles). The black open circles represent resistances measured after releasing the strain. The inset shows a photograph of the sample during the bending test.

We also applied the one-step micropatterning technique to fabricate the 144 element multitouch projected capacitive sensors. A projected capacitive touch sensor is composed of two conductive layers for x- and y-axes, comprising interlocking diamond-shaped electrodes, separated by an insulator as shown in Figure 6a. In the case of conventional touch sensors using ITO, several steps and vacuum processes are necessary to form the diamond-shaped electrode arrays: (1) vacuum sputtering of ITO on the entire surface of a substrate, (2) photolithography (spin-coating of photoresist, exposure, and development), (3) wet etching and rinse, and (4) removal of the photoresist. In contrast, the present micropatterning technique can form the electrode arrays of CNT films by a nonvacuum, room-temperature, one-step process, demonstrating energy- and material-saving production of low-cost, high-performance touch sensors.

Figure 6b shows a schematic of the fabrication process. Similar to the microgrid TCFs described above, CNTs exhausted from the FC-CVD process were collected with a membrane filter (Millipore HVHP14250, PVDF with 0.45 μm pores) with resist patterns for the 12 $\times$ 12 diamond-shaped electrodes (see Figure S5 in Supporting Information for the patterns) and then

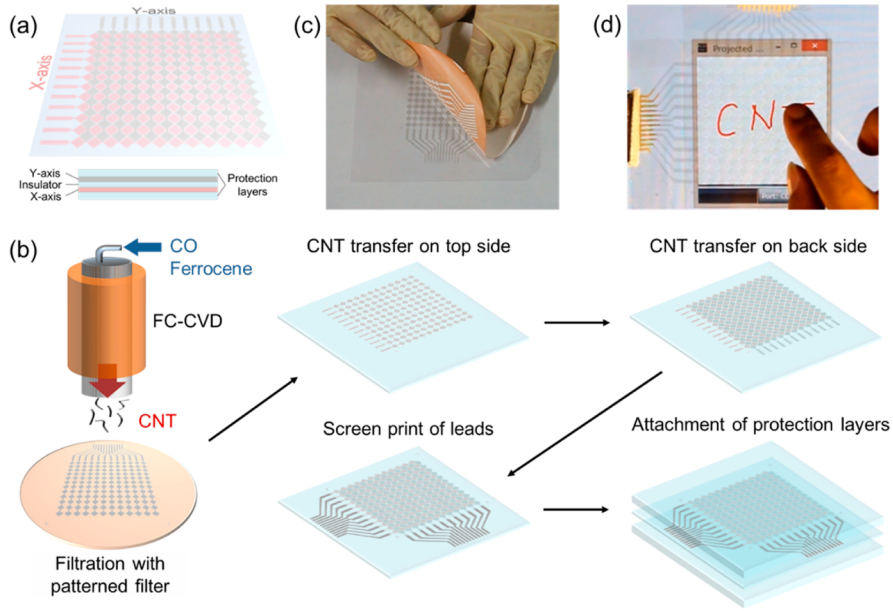

Figure 6. (a) Schematic of a multitouch projected capacitive sensor, which is composed of two conductive layers separated by an insulator. Each conductive layer consists of interlocking diamond-shaped electrodes. (b) Schematic of the fabrication process for a capacitive touch sensor. CNTs exhausted from the FC-CVD process are collected by the patterned membrane filter and then transferred onto both sides of a thin PEN substrate. After screen printing of Ag paste to form leads, protection layers are attached on both sides. Photographs taken during (c) the transfer process and (d) touch sensor operation on an LCD monitor.

transferred from the membrane filter onto both sides of an insulator, as shown in Figure 6c (a movie S2 is also available in Supporting Information). We used a PEN film with a thickness of 50 μm (Teijin DuPont Films, Q65HA) as the insulator layer. After densification and chemical doping of the CNT films, leads were formed with silver paste (Sigma-Aldrich, silver paste DGP80 TESM8020) by the screen-printing technique. Finally, the protection films (100 μm thick PEN films) were attached to both sides. The CNT growth condition, fabrication process of the patterned filter, conditions of densification, and chemical doping processes are same as for the microgrids described above. All fabrication processes were carried out under ambient conditions. The touch sensor was connected to the driver circuit, which was connected to a PC *via* a USB (see Methods section).

The transmittances of the CNT layer and overall touch sensor were 90.5 and 77.6%, respectively, at a wavelength of 550 nm. The overall transmittance could be improved by suppressing reflection at the surface of the protection layers by laminating an antireflection layer over the surface. Figure 6d shows a photograph demonstrating an operation of the 7 $\times$ 7 cm^2 touch sensor on an LCD monitor of a laptop PC. In addition to writing words, multitouch actions were successfully demonstrated with the current CNT touch sensor (see movie S3 in Supporting Information). Even though there was a finite resistance of about 30 MΩ between neighboring electrodes due to the CNTs deposited on the photoresist during the filtration process, the conductivity is negligible in the operation of the touch sensor because the resistance is 3 orders of magnitude larger than the resistance of series of an interlocking electrode array of about 40 kΩ.

CONCLUSION

In conclusion, we developed a technique for one-step micropatterning of as-grown CNT films on a plastic substrate based on the dry transfer process, using the patterned membrane filter on which resist patterns were formed. This technique enabled quick and ambient fabrication of sub-10 μm CNT patterns with 100% utilization of the CNT material. By utilizing this technique, we obtained a high-performance CNT transparent conductive film with a microgrid structure. The sheet resistance was reduced by a maximum of 46% by adding the microgrid, leading to a value of 53 Ω/sq at a transmittance of 80% over the trade-off between the sheet resistance and transmittance of conventional uniform CNT TCFs. Further improvements in transmittance and sheet resistance would be possible by increasing the aperture ratio. We also demonstrated easy fabrication of multitouch projected capacitive sensors with 12 $\times$ 12 electrodes. These results show that the micropatterning technique developed in this work is quite useful to manufacture high-performance, rare-metal-free, ultra-low-cost transparent conductor devices.

METHODS

CNT Growth. CNTs were grown by an ambient-pressure FC-CVD technique with CO as the carbon source,[30] wherein catalyst nanoparticles were produced by the decomposition of ferrocene vapor. CO (100 sccm) was passed through a cartridge containing ferrocene powder. Additional CO (400 sccm) and CO_2 (3 sccm) was introduced into the furnace. The growth temperature was 850 °C. The CNTs were characterized by absorption and Raman scattering spectroscopies that showed that the mean diameter of the CNTs was 1.35 nm and the ratio of G-band and D-band intensities (G/D ratio) was 14.6 (Supporting Information Figure S6).

Lithography on the Membrane Filter. CF_4 plasma was exposed to the membrane filter at a radio frequency power of 50 W for 120 s in order to enhance hydrophobicity of the membrane filter. Photoresist (Shipley, S1813G) was spin-coated at 5000 rpm for 50 s. The thickness of the photoresist was 1 μm. The UV exposure and development were carried out with the standard conditions for S1813G.

Raman Scattering Spectroscopy. Micro-Raman scattering spectroscopy was performed using a Renishaw InVia confocal Raman spectrometer with a 532 nm laser source. The laser spot was focused on about 1 μm in diameter on the sample surface with an objective lens (50×). For the mapping measurement, the motor-driven stage was scanned every 2 μm with PC control.

Densification and Chemical Doping. Densification was performed by soaking the sample in IPA for 60 s and then drying with N_2. The CNT film was densified by the surface tension of IPA when IPA was evaporated. Chemical doping was carried out by soaking the sample in HNO_3 for 60 s and rinsing with water. See Figure S7 in Supporting Information for the variation in performance of the CNT TCF with the microgrid with densification and chemical doping.

Touch Sensor Operation. We used a commercially available kit (Microchip, DM160211) for the operation of the fabricated CNT touch sensor. We also used the software bundled with the kit (Projected Capacitive Demo 1.08) to adjust parameters for the operation and demonstrate the operation of the touch sensor.

Conflict of Interest: The authors declare no competing financial interest.

Acknowledgment. Y.O. thanks Prof. Esko I. Kauppinen of Aalto University for instructing FC-CVD technique and valuable discussions. This work was partially supported by the Advanced Low Carbon Technology Research and Development Program (ALCA) and Strategic International Collaborative Research Program (SICORP) of Japan Science and Technology Agency, and a Grant-in-Aid for Scientific Research of Japan Society for the Promotion of Science.

Supporting Information Available: Movie showing one-step micropatterning of CNTs on plastic film; reusability of patterned membrane filter; validity of expression for sheet resistance of CNT TCFs with a microgrid structure, evaluation of absorption coefficient and resistivity of CNT film; comparison between experimental results and models for sheet resistance and transmittance, pattern of diamond-shaped electrodes for touch sensor; movie showing one-step formation of electrode array for multitouch projected capacitive sensor; movie demonstrating the operation of touch sensor; absorption and Raman scattering spectra of as-grown CNTs; variations in transmittance and sheet resistance with densification and chemical doping. This material is available free of charge *via* the Internet at http://pubs.acs.org.

REFERENCES AND NOTES

1. Wu, Z. C.; Chen, Z. H.; Du, X.; Logan, J. M.; Sippel, J.; Nikolou, M.; Kamaras, K.; Reynolds, J. R.; Tanner, D. B.; Hebard, A. F.; *et al.* Transparent, Conductive Carbon Nanotube Films. *Science* **2004**, *305*, 1273–1276.
2. Hu, L.; Hecht, D. S.; Gruner, G. Percolation in Transparent and Conducting Carbon Nanotube Networks. *Nano Lett.* **2004**, *4*, 2513–2517.
3. Kaempgen, M.; Duesberg, G. S.; Roth, S. Transparent Carbon Nanotube Coatings. *Appl. Surf. Sci.* **2005**, *252*, 425–429.
4. Gruner, G. Carbon Nanotube Films for Transparent and Plastic Electronics. *J. Mater. Chem.* **2006**, *16*, 3533–3539.
5. Geng, H. Z.; Kim, K. K.; So, K. P.; Lee, Y. S.; Chang, Y.; Lee, Y. H. Effect of Acid Treatment on Carbon Nanotube-Based Flexible Transparent Conducting Films. *J. Am. Chem. Soc.* **2007**, *129*, 7758–7759.
6. Dan, B.; Irvin, G. C.; Pasquali, M. Continuous and Scalable Fabrication of Transparent Conducting Carbon Nanotube Films. *ACS Nano* **2009**, *3*, 835–843.
7. Kaskela, A.; Nasibulin, A. G.; Timmermans, M. Y.; Aitchison, B.; Papadimitratos, A.; Tian, Y.; Zhu, Z.; Jiang, H.; Brown, D. P.; Zakhidov, A.; *et al.* Aerosol-Synthesized SWCNT Networks with Tunable Conductivity and Transparency by a Dry Transfer Technique. *Nano Lett.* **2010**, *10*, 4349–4355.
8. Purewal, M. S.; Hong, B. H.; Ravi, A.; Chandra, B.; Hone, J.; Kim, P. Scaling of Resistance and Electron Mean Free Path of Single-Walled Carbon Nanotubes. *Phys. Rev. Lett.* **2007**, *98*, 186808.
9. Perebeinos, V.; Tersoff, J.; Avouris, P. Electron−Phonon Interaction and Transport in Semiconducting Carbon Nanotubes. *Phys. Rev. Lett.* **2005**, *94*, 086802.
10. Segal, M. Selling Graphene by the Ton. *Nat. Nanotechnol* **2009**, *4*, 612–614.
11. Iijima, S.; Brabec, C.; Maiti, A.; Bernholc, J. Structural Flexibility of Carbon Nanotubes. *J. Chem. Phys.* **1996**, *104*, 2089–2092.
12. Hecht, D. S.; Thomas, D.; Hu, L. B.; Ladous, C.; Lam, T.; Park, Y.; Irvin, G.; Drzaic, P. Carbon-Nanotube Film on Plastic as Transparent Electrode for Resistive Touch Screens. *J. Soc. Inf. Display* **2009**, *17*, 941–946.
13. Cao, Q.; Kim, H. S.; Pimparkar, N.; Kulkarni, J. P.; Wang, C. J.; Shim, M.; Roy, K.; Alam, M. A.; Rogers, J. A. Medium-Scale Carbon Nanotube Thin-Film Integrated Circuits on Flexible Plastic Substrates. *Nature* **2008**, *454*, 495–500.
14. Sun, D. M.; Timmermans, M. Y.; Tian, Y.; Nasibulin, A. G.; Kauppinen, E. I.; Kishimoto, S.; Mizutani, T.; Ohno, Y. Flexible High-Performance Carbon Nanotube Integrated Circuits. *Nat. Nanotechnol.* **2011**, *6*, 156–161.
15. Sun, D. M.; Timmermans, M. Y.; Kaskela, A.; Nasibulin, A. G.; Kishimoto, S.; Mizutani, T.; Kauppinen, E. I.; Ohno, Y. Mouldable All-Carbon Integrated Circucits. *Nat. Commun.* **2013**, *4*, 2302.
16. Novoselov, K. S.; Geim, A. K.; Morozov, S. V.; Jiang, D.; Katsnelson, M. I.; Grigorieva, I. V.; Dubonos, S. V.; Firsov, A. A. Two-Dimensional Gas of Massless Dirac Fermions in Graphene. *Nature* **2005**, *438*, 197–200.
17. Geim, A. K. Graphene: Status and Prospects. *Science* **2009**, *324*, 1530–1534.
18. Li, X. S.; Zhu, Y. W.; Cai, W. W.; Borysiak, M.; Han, B. Y.; Chen, D.; Piner, R. D.; Colombo, L.; Ruoff, R. S. Transfer of Large-Area Graphene Films for High-Performance Transparent Conductive Electrodes. *Nano Lett.* **2009**, *9*, 4359–4363.
19. Bae, S.; Kim, H.; Lee, Y.; Xu, X. F.; Park, J. S.; Zheng, Y.; Balakrishnan, J.; Lei, T.; Kim, H. R.; Song, Y. I.; *et al.* Roll-to-Roll Production of 30-Inch Graphene Films for Transparent Electrodes. *Nat. Nanotechnol.* **2010**, *5*, 574–578.
20. Meitl, M. A.; Zhou, Y. X.; Gaur, A.; Jeon, S.; Usrey, M. L.; Strano, M. S.; Rogers, J. A. Solution Casting and Transfer Printing Single-Walled Carbon Nanotube Films. *Nano Lett.* **2004**, *4*, 1643–1647.
21. Jo, J. W.; Jung, J. W.; Lee, J. U.; Jo, W. H. Fabrication of Highly Conductive and Transparent Thin Films from Single-Walled Carbon Nanotubes Using a New Non-ionic Surfactant *via* Spin Coating. *ACS Nano* **2010**, *4*, 5382–5388.
22. Nasibulin, A. G.; Kaskela, A.; Mustonen, K.; Anisimov, A. S.; Ruiz, V.; Kivisto, S.; Rackauskas, S.; Timmermans, M. Y.; Pudas, M.; Aitchison, B.; *et al.* Multifunctional Free-Standing Single-Walled Carbon Nanotube Films. *ACS Nano* **2011**, *5*, 3214–3221.
23. Kim, H.; Horwitz, J. S.; Kushto, G. P.; Kafafi, Z. H.; Chrisey, D. B. Indium Tin Oxide Thin Films Grown on Flexible Plastic Substrates by Pulsed-Laser Deposition for Organic Light-Emitting Diodes. *Appl. Phys. Lett.* **2001**, *79*, 284–286.
24. Wong, F. L.; Fung, M. K.; Tong, S. W.; Lee, C. S.; Lee, S. T. Flexible Organic Light-Emitting Device Based on Magnetron Sputtered Indium-Tin-Oxide on Plastic Substrate. *Thin Solid Films* **2004**, *466*, 225–230.
25. Lee, J. Y.; Connor, S. T.; Cui, Y.; Peumans, P. Solution-Processed Metal Nanowire Mesh Transparent Electrodes. *Nano Lett.* **2008**, *8*, 689–692.
26. Fuhrer, M. S.; Nygard, J.; Shih, L.; Forero, M.; Yoon, Y. G.; Mazzoni, M. S. C.; Choi, H. J.; Ihm, J.; Louie, S. G.; Zettl, A.; *et al.* Crossed Nanotube Junctions. *Science* **2000**, *288*, 494–497.
27. Nirmalraj, P. N.; Lyons, P. E.; De, S.; Coleman, J. N.; Boland, J. J. Electrical Connectivity in Single-Walled Carbon Nanotube Networks. *Nano Lett.* **2009**, *9*, 3890–3895.
28. Stadermann, M.; Papadakis, S. J.; Falvo, M. R.; Novak, J.; Snow, E.; Fu, Q.; Liu, J.; Fridman, Y.; Boland, J. J.; Superfine, R.; *et al.* Nanoscale Study of Conduction through Carbon Nanotube Networks. *Phys. Rev. B* **2004**, *69*, 201402.
29. Znidarsic, A.; Kaskela, A.; Laiho, P.; Gaberscek, M.; Ohno, Y.; Nasibulin, A. G.; Kauppinen, E. I.; Hassanien, A. Spatially Resolved Transport Properties of Pristine and Doped Single-Walled Carbon Nanotube Networks. *J. Phys. Chem. C* **2013**, *117*, 13324–13330.
30. Moisala, A.; Nasibulin, A. G.; Brown, D. P.; Jiang, H.; Khriachtchev, L.; Kauppinen, E. I. Single-Walled Carbon Nanotube Synthesis Using Ferrocene and Iron Pentacarbonyl in a Laminar Flow Reactor. *Chem. Eng. Sci.* **2006**, *61*, 4393–4402.
31. Cao, Q.; Zhu, Z. T.; Lemaitre, M. G.; Xia, M. G.; Shim, M.; Rogers, J. A. Transparent Flexible Organic Thin-Film Transistors That Use Printed Single-Walled Carbon Nanotube Electrodes. *Appl. Phys. Lett.* **2006**, *88*, 113511.
32. Liu, Y. M.; Liu, L.; Liu, P.; Sheng, L. M.; Fan, S. S. Plasma Etching Carbon Nanotube Arrays and the Field Emission Properties. *Diamond Relat. Mater.* **2004**, *13*, 1609–1613.
33. Gu, Z. N.; Shaver, J.; Hauge, R. H.; Smalley, R. E.; Margrave, J. L. Room Temperature Oxidative Etching and/or Cutting of Single-Walled Carbon Nanotubes by Ozone. *Abstr. Pap., Am. Chem. Soc.* **2003**, *226*, U714.
34. Mawhinney, D. B.; Naumenko, V.; Kuznetsova, A.; Yates, J. T.; Liu, J.; Smalley, R. E. Infrared Spectral Evidence for the Etching of Carbon Nanotubes: Ozone Oxidation at 298 K. *J. Am. Chem. Soc.* **2000**, *122*, 2383–2384.
35. Byl, O.; Liu, J.; Yates, J. T. Etching of Carbon Nanotubes by Ozone—A Surface Area Study. *Langmuir* **2005**, *21*, 4200–4204.
36. Zhou, Y. X.; Hu, L. B.; Gruner, G. A Method of Printing Carbon Nanotube Thin Films. *Appl. Phys. Lett.* **2006**, *88*, 123109.
37. Wang, J.; Musameh, M. Carbon Nanotube Screen-Printed Electrochemical Sensors. *Analyst* **2004**, *129*, 1–2.
38. Kordas, K.; Mustonen, T.; Toth, G.; Jantunen, H.; Lajunen, M.; Soldano, C.; Talapatra, S.; Kar, S.; Vajtai, R.; Ajayan, P. M. Inkjet Printing of Electrically Conductive Patterns of Carbon Nanotubes. *Small* **2006**, *2*, 1021–1025.
39. Vaillancourt, J.; Zhang, H.; Vasinajindakaw, P.; Xia, H.; Lu, X.; Han, X.; Janzen, D. C.; Shih, W.-S.; Jones, C. S.; Stroder, M.; *et al.* All Ink-Jet-Printed Carbon Nanotube Thin-Film Transistor on a Polyimide Substrate with an Ultrahigh Operating Frequency of over 5 GHz. *Appl. Phys. Lett.* **2008**, *93*, 243301.
40. Okimoto, H.; Takenobu, T.; Yanagi, K.; Miyata, Y.; Shimotani, H.; Kataura, H.; Iwasa, Y. Tunable Carbon Nanotube Thin-Film Transistors Produced Exclusively *via* Inkjet Printing. *Adv. Mater.* **2010**, *22*, 3981–3986.

41. Lim, C. H.; Min, D. H.; Lee, S. B. Direct Patterning of Carbon Nanotube Network Devices by Selective Vacuum Filtration. *Appl. Phys. Lett.* **2007**, *91*, 243117.
42. Timmermans, M. Y.; Grigoras, K.; Nasibulin, A. G.; Hurskainen, V.; Franssila, S.; Ermolov, V.; Kauppinen, E. I. Lithography-Free Fabrication of Carbon Nanotube Network Transistors. *Nanotechnology* **2011**, *22*, 065303.
43. Yim, J. H.; Kim, Y. S.; Koh, K. H.; Lee, S. Fabrication of Transparent Single Wall Carbon Nanotube Films with Low Sheet Resistance. *J. Vac. Sci. Technol., B* **2008**, *26*, 851–855.
44. Green, A. A.; Hersam, M. C. Processing and Properties of Highly Enriched Double-Wall Carbon Nanotubes. *Nat. Nanotechnol.* **2009**, *4*, 64–70.
45. Hecht, D. S.; Heintz, A. M.; Lee, R.; Hu, L. B.; Moore, B.; Cucksey, C.; Risser, S. High Conductivity Transparent Carbon Nanotube Films Deposited from Superacid. *Nanotechnology* **2011**, *22*, 169501.
46. Suo, Z.; Ma, E. Y.; Gleskova, H.; Wagner, S. Mechanics of Rollable and Foldable Film-on-Foil Electronics. *Appl. Phys. Lett.* **1999**, *74*, 1177–1179.
47. Trottier, C. M.; Glatkowski, P.; Wallis, P.; Luo, J. Properties and Characterization of Carbon-Nanotube-Based Transparent Conductive Coating. *J. Soc. Inf. Display* **2005**, *13*, 759–763.